The impact of methane thermodynamics on seasonal convection and circulation in a model Titan atmosphere

Jonathan L. Mitchell

Institute for Advanced Study, Princeton, NJ 08540

mitch@ias.edu

Raymond T. Pierrehumbert

Department of Geophysical Sciences, The University of Chicago, Chicago, IL 60637

Dargan M. W. Frierson

Department of Atmospheric Sciences, The University of Washington, Seattle, WA

Rodrigo Caballero

School of Mathematical Sciences, University College Dublin, Dublin, Ireland

Received _____; accepted _____

52 pages, 9 figures, 5 tables

ABSTRACT

We identify mechanisms controlling the distribution of methane convection and large-scale circulation in a simplified, axisymmetric model atmosphere of Titan forced by gray radiation and moist (methane) convection. The large-scale overturning circulation, or Hadley cell, is global in latitudinal extent and provides fundamental control of precipitation and tropospheric winds. The precipitating, large-scale updraft regularly oscillates in latitude with seasons. The distance of greatest poleward excursion of the Hadley cell updraft is set by the mass of the convective layer of the atmosphere; convection efficiently communicates seasonal warming of the surface through the cold and dense lower atmosphere, increasing the heat capacity of the system. The presence of deep, precipitating convection introduces three effects relative to the case with no methane latent heating: 1) convection is narrowed and enhanced in the large-scale updraft of the Hadley cell; 2) the latitudinal amplitude of Hadley cell updraft oscillations is decreased; and 3) a time lag is introduced. These effects are observable in the location and timing of convective methane clouds in Titan's atmosphere as a function of season. A comparison of simulations over a range of convective regimes with available observations suggest methane thermodynamic-dynamic feedback is important in the Titan climate.

Subject headings: TITAN; ATMOSPHERES, DYNAMICS

1. Introduction

Clouds evolving on short (presumably convective) timescales have been observed in the lowest 40 km of Titan's atmosphere (*Griffith et al.* (2005)). *Barth and Rafkin* (2007) showed the Huygens temperature and methane concentration profiles would not allow for energetic convection like that observed to occur. The primary reason is that since the methane concentration near the surface is well below saturation, there is very little convective available potential energy (CAPE) to be released. The large-scale circulation can locally enhance the methane concentration by focusing the latent energy of methane vapor to a particular latitude. This focusing process is not captured in models which ignore the large-scale fluid motion of the atmosphere.

Latitudinal temperature gradients drive a meridional overturning circulation, or Hadley cell, that greatly reduces latitudinal temperature gradients in its region of influence. The resulting thermally homogenized zone defines, in a dynamical sense, the tropics. Steady axisymmetric theories of tropical dynamics utilize the rotational coupling of horizontal temperature gradients and vertical wind shear together with angular momentum conservation to determine the latitudinal width of the Hadley cell zone, φ_H. The predicted width scales as $\varphi_H \propto \sqrt{gH}/(\Omega a)$, where φ_H is the latitudinal extent of the a Hadley circulation that is symmetric about the equator, g is the surface gravity, Ω is the planetary rotation rate, a is the planetary radius, and H is the atmosphere scale-height (*Held and Hou* 1980; *Caballero et al.* 2008). The theory leads to the conclusion that Titan's Hadley cells span the globe. Titan is globally tropical by Earth standards, so our understanding of atmospheric phenomena in Earth's tropics can be used to interpret observations of Titan.

Steady theories are perhaps more relevant to Earth because the thermal inertia of the oceans are able to integrate out much of the seasonal cycle. The surface of Titan, however, is devoid of any large reservoirs of liquid, and 20% of the surface is covered

with dunes (*Lorenz et al.* 2008; *Lorenz et al.* 2006). Titan's solid surface has low heat capacity and weak thermal inertia and could respond very quickly to even modest changes in insolation. *Tokano* (2005) assessed the effect of different surface types on the seasonal cycle of the large-scale circulation in a dry (no methane thermodynamics) model Titan atmosphere (general circulation model, or GCM). All surface types used had thermal inertia orders of magnitude less than the atmospheric thermal inertia. Consequently, the models produced large surface temperature variations, and the lowest portion of the atmosphere, corresponding to the depth of the dry convective layer (∼1500–1000 hPa), also showed large seasonal variation.

It was originally thought the lower atmosphere of Titan would respond steadily to the annual-mean insolation, since the thermal inertia of the atmosphere is larger than the length of a Titan year (*Flasar et al.* (1981)). If we focus on the lowest 40 km, the region below the cold trap, the radiative timescale $\tau_{rad} \sim 180$ years, many times the length of a season (29.5 Earth years). Were convection to persistently penetrate the depth of the troposphere, the atmosphere would cool on this timescale which would average out a significant fraction of the seasonal cycle. However, if convection only warms the lowest 5-10 km ($\sim$ 500 hPa) of the atmosphere – as would be expected for dry convection – τ_{rad} is within a factor of two of the seasonal period. In this regime, one can expect large seasonal variations in the troposphere. We will return to this discussion in Section 3.4.1.

Observations of methane clouds in Titan's southern hemisphere cannot be explained by a steady, equatorially symmetric circulation in the lower atmosphere, which would concentrate clouds at the equator. The majority of clouds have been observed directly over the southern pole, which recently experienced summer solstice (see e.g. *Brown et al.* (2002); *Bouchez and Brown* (2005); *Schaller et al.* (2006a); *Hirtzig et al.* (2006, 2007)). Mid-latitude clouds occasionally occur, but again only in the southern hemisphere (*Roe*

et al. 2005; *Griffith et al.* 2005). The recent dissipation and paucity of the south-polar clouds suggests the lower atmosphere experiences significant seasonal variability (*Schaller et al.* 2006b).

While cloud-resolving models like those reported in *Hueso and Sanchez-Lavega* (2006) and *Barth and Rafkin* (2007) can produce vigorous convective storms, the incorporation of methane thermodynamics in circulation models of Titan's atmosphere has led to mixed conclusions. *Tokano et al.* (2001) found that in simulations with fixed surface temperature and a fixed but limited availability of surface methane (equivalent to forcing the first layer of the atmosphere towards 50% relative humidity), the atmosphere is sensitive to the saturation condition for grid-scale condensation. The latent heating by methane condensation was found to have negligible effect on the vertical temperature profile. *Rannou et al.* (2006) similarly fixed the surface methane availability to 50% in a fully seasonal, two-dimensional model Titan atmosphere which included more sophisticated parameterizations for methane cloud formation. They found the observed latitudinal distribution of clouds results from large-scale motions in the atmosphere, and they also concluded that methane thermodynamics has a negligible effect on the vertical temperature structure. *Mitchell et al.* (2006) showed methane thermodynamics can have a profound effect on the latitudinal distribution of precipitating convection and the associated circulation in an axisymmetric model Titan atmosphere, and they conclude methane is important in making model predictions consistent with observed cloud patterns. *Mitchell* (2008) explored the sensitivity of low-latitude surface drying to the assumed total reservoir of methane and found strong feedbacks between methane thermodynamics and surface climatology.

A primary motivating question of the current study is: Does methane thermodynamics play a role in the seasonal character of Titan's lower atmosphere? In this paper, we study the cases first presented in *Mitchell et al.* (2006), but with a more realistic radiative scheme,

and spell out in detail the feedbacks of methane thermodynamics on Titan's atmosphere. We describe the model in Section 2, give a detailed analysis of the results in Section 3, and offer conclusions in Section 4.

2. Model description

Here we describe the components of our atmospheric model. For a summary of the model parameters discussed in the following section, see Table 1.

[**Table 1**]

As in *Mitchell* (2008), we use the axisymmetric primitive equations to model the fluid flow of the atmosphere (*Vallis* 2006). We discretize the equations on a regular grid in pressure and latitude, with 27 pressure levels and 45 latitude cells. We apply a numerical smoother in the horizontal to the meridional velocities; the operator is equivalent to a second-order diffusion. The smoothing filters out much of the variability of the 2D dynamical core, which results from numerical instability. These simplifications allow us to model the overall character of the large-scale circulation in a reasonable amount of computational time. We make no attempt to model the mixing effect of large-scale eddies on momentum; by doing so, we exclude the development of superrotation.

We use a simplified, flexible suite of atmospheric physics developed for general planetary applications. The most novel feature of the model is the inclusion of a moist convection scheme; all previous global Titan models assumed condensation is resolved at the grid scale, which introduces resolution sensitivity to the model and underestimates the vigor of convective updrafts, since these motions are non-hydrostatic. We employ a simplified Betts-Miller moist convection scheme, which is described in detail in *Frierson* (2007). Briefly, the scheme relaxes moisture to a specified relative humidity and temperatures to the

moist adiabat at a specified timescale when there is CAPE. There are only two parameters in the scheme, the relaxation timescale, τ_{BM}, which we always fix at 2 hours, and the target relative humidity, rh_{BM}, which we vary in our simulations in the range 0.4 to 0.8. The relative humidity parameter determines the precipitation efficiency of the convection; for a given amount of CAPE, a lower(higher) value of rh_{BM} releases a higher(lower) amount of energy via condensation. Though originally developed for application to Earth, the scheme is sufficiently flexible to be used for any condensible substance. In this and all other model components, we assume the saturation vapor pressure of methane follows the Clausius-Clapeyron relation. We do not explicitly take into account the ∼20% depression of the vapor pressure or 10% increase in the latent heat of vaporization by the presence of dissolved nitrogen (*Thompson et al.* 1992), nor do we consider the possibility of convective momentum transport, which is not easily considered in a Betts-Miller-type convection scheme. The former, thermodynamic effect could be important to cloud development in regions with subsaturated air near the surface, as pointed out by *Barth and Rafkin* (2007).

Radiative transfer is solved by assuming the infrared absorptivity of the atmosphere is independent of frequency and the absorbers are uniformly mixed in the column. We neglect the radiative feedback of methane in order to isolate its thermodynamic effects. Direct absorption of solar shortwave radiation in the atmosphere is treated parametrically and is fixed in all simulations. For a more complete description of the radiative scheme, see *Mitchell* (2008).

The surface temperature is self-consistently prognosed according to energy fluxes at the surface-atmosphere boundary which include radiative, sensible (dry) heat, and latent heat fluxes. The change in surface temperature is inferred by assuming a fixed, uniform heat capacity (per unit area) of the order of 2×10^5 J/m^2/K, which is near the value assigned

to a "porous icy regolith" in *Tokano* (2005).[1] While this heat capacity is low for putative hydrocarbon lakes (*Tokano* 2005), the heat capacity of the atmosphere is at least an order of magnitude larger. Surface fluxes are diagnosed in the manner specified in *Mitchell* (2008), except for the latent fluxes which we diagnose as follow:

$$F_{lat} = \begin{cases} -C_d \rho U L_v (r h_s q_s - q_0) & \rho_s < \rho_0 \\ -C_d \rho U L_v (r h_s q_s - q_0) e^{-\frac{(\rho_s - \rho_0)}{\rho_e}} & \rho_s > \rho_0, \end{cases} \tag{1}$$

where, C_d is a bulk exchange coefficient, U is a parameter representing the surface wind, L_v is the latent heat of vaporization, rh_s is the target relative humidity of the surface-level air, q_s is the saturation mass mixing ratio of methane at the surface temperature, q_0 is the mass mixing ratio of methane at the temperature of surface-level air ($\sim$700 m), ρ_s is the density of saturated air at the surface temperature, ρ_0 is the density of surface-level air, ρ_e is a specified e-folding parameter, and C_p is the specific heat of nitrogen. The exponential factor is intended to qualitatively model the attenuation of fluxes in the presence of a temperature inversion since turbulent exchange cannot efficiently operate in a stable environment. The linearized aerodynamic formula, Eq. 1, would otherwise predict large, compensating fluxes of sensible and latent energy, which is an unphysical application of the linear formula.

Vertical mixing of moisture and momentum in the boundary layer is modeled with a fixed diffusion coefficient, ν, and fixed layer depth (1500-1000 mbar) with the form

$$\left(\frac{\partial}{\partial t}\right)_{diff} = \frac{\partial}{\partial p}\left(\nu g^2 \rho^2 \frac{\partial}{\partial p}\right) . \tag{2}$$

There is no vertical diffusion above the boundary layer. We fix the diffusion coefficient $\nu = 10^{-2}$ m^2/s.

---

[1]This heat capacity corresponds to a timescale of 10 Earth days for a surface radiating at 95 K.

3. Results

As in *Mitchell et al.* (2006), we explore the sensitivity of our model to a range of regimes from "moist", i.e. the effects of methane thermodynamics included, to "dry"; parameters differing between the cases are summarized in Table 2. We vary the parameters that control the methane vapor concentration in the atmosphere and the latent heat of condensation/evaporation of methane. We focus attention on three representative cases. First, we perform a "moist" simulation with unrestricted methane supply from the surface ($rh_s = 1$) and a high relative humidity threshold for convection to occur ($rh_{BM} = 0.8$). In the "dry" simulation, we artificially remove the latent heat from methane condensation and evaporation by setting $L_v = 0$ while keeping the other parameters fixed. It is important to note that in the dry case, the latent heat is set to zero in every model component, which is necessary to keep the model energetically closed; the flux of methane vapor in the atmosphere is also closed, but does not have physical meaning. The dry case should not be thought of as a real planet, rather a convenient way to model one end member of our idealized simulations. Finally, we perform an "intermediate" simulation in which we uniformly restrict the methane supply at the surface by setting $rh_s = 0.5$, and we set $rh_{BM} = 0.4$; reducing rh_{BM} increases the convection efficiency, i.e. convective energy is more readily released by moist convection rather than dry convection than for higher values of rh_{BM}. We compare the mass streamfuction, zonal winds, and angular momentum transport of these cases in Sections 3.1 and 3.2. We then compare model diagnostics with available observations in Section 3.3.

[**Table 2**]

3.1. Mass streamfunction and zonal winds

Figure 1 shows the instantaneous mass streamfunction in petagrams/s for our *moist* simulation at the four seasons. The difference between adjacent contours of the mass streamfunction represents the mass flux in that region; positive values (warm colors) are rotating clockwise and negative values (cool colors) are rotating counter-clockwise. It is clear from these plots that the Hadley cell is not steady, but rather oscillates with the seasonal forcing. This oscillation is reminiscent of the situation of Earth, where the Hadley cell also shows significant seasonal variability (Lindzen+Hou 1988). However, the seasonality is much more extreme on Titan; the difference is attributable to the large heat capacity and thermal inertia of Earth's oceans. There is also a significant time lag evident in the seasonal response of Titan's Hadley cell; the large-scale updraft is further poleward at both equinoxes relative to the solstices. The maximum latitude reached by the updraft in the moist case occurs between the solstices and equinoxes (see Section 3.3.1). [**Figure 1**]

Since the Huygens probe landed on Titan shortly following southern summer solstice (SSS), we now provide more details of our simulations during this season. Figure 2 shows the mass streamfunctions, or Hadley circulations (left column), and zonal winds (right column) at SSS for our three simulations; the units of the former are petagrams/s and the latter are m/s. Positive zonal winds (warm colors) are flowing west-to-east and are referred to as westerlies, and negative winds (cool colors) are flowing east-to-west and are called easterlies.

In the moist case (top row of Figure 2), the winter (cross-equatorial) Hadley cell spans from mid-latitudes in the summer hemisphere to the winter pole. The streamlines are more densely packed in the updraft of the winter cell than the downdraft, which is the mark of a moist-convective updraft, or Inter-tropical Convergence Zone (ITCZ). The summer cell is very weak and transient; variability in the circulation tends to mask a coherent summer

Hadley cell. The zonal winds show double-jet structure with a winter jet at 70N and a summer jet at 70S. Easterlies prevail in the region between the jets and altitudes below 200 hPa, which is roughly the tropopause.[2] Easterlies aloft along the poleward branch of the winter Hadley circulation are the result of angular momentum conservation following the flow.

The second row of Fig. 2 displays model winds at SSS in the dry case, with the latent heat of methane removed. The Hadley circulation in this case is confined primarily to levels below 1000 hPa, which corresponds roughly to 9 km. The cell has roughly equal areas of upwelling and downwelling which reflects the lack of latent heating in the updraft. The circulation is vigorous, roughly 5 times stronger than the moist case. It is somewhat remarkable that the Hadley cell is so much stronger in the case with no latent heat release, as condensation provides a large energy source for the circulation. In fact, it is often stated that the Earth's Hadley cell is "driven", or greatly enhanced, by latent heat release. To reconcile this viewpoint with our simulation results, it is important to consider the effect of moisture on determining the static stability of the atmosphere. In the dry case, the conditions in the convective layer are nearly neutral, and therefore the mass flux can become quite large in order to produce the heat flux needed to sustain uniform temperatures in the Hadley domain. In the moist cases, on the other hand, the static stability is quite larger in the subtropics, which requires a more modest circulation. For axisymmetric solutions of dry Hadley cells and scaling laws for the strength of the circulation in the dry limit, see *Caballero et al.* (2008); for more discussion on the sensitivity of the Hadley circulation to moisture content, see *Frierson et al.* (2006).

In the dry case there is a single, pole-to-pole circulation that is in-phase with the solar

[2]Zonal winds above 200 hPa should not be considered realistic since our radiative scheme does not reproduce the observed stratospheric temperatures.

forcing, i.e. the updraft of the Hadley cell coincides with the maximum solar forcing. The zonal winds in this case show a more complicated structure. The region below 1000 hPa has a single, somewhat distinct winter jet at 60N latitude; this is the jet produced by the angular momentum transport of the pole-to-pole Hadley circulation. The Hadley cell in the dry case is vigorous enough to essentially instantaneously affect zonal winds (see Section 3.2). Winds along the poleward branch of the Hadley cell from the south pole to 50N are easterly, as expected from angular momentum conservation with a high-latitude updraft. In the region between 1000 and the top of the domain, there are two isolated jets at 70N and 70S, while winds at low latitudes are again easterly. The mass flux in this region is at least two orders of magnitude less vigorous as in the convective layer, and the double jet structure reflects hemispherically symmetric, annual average overturning circulation (see Figure 4(e)). The region between 200 hPa and 1000 hPa is dynamically distinct from both the stratosphere, which is usually referred to as being above the temperature minimum at 200 hPa, and the convective Hadley cell, which in the current case is isolated to altitudes below 1000 hPa.

The third row of Fig. 2 shows the model winds at SSS for the intermediate case. The Hadley circulation is a hybrid of the moist and dry cases; in magnitude, the mass flux is roughly double the moist case and half the dry case below 1000 hPa and a weaker branch extends into the 1000 to 200 hPa region. A single pole-to-pole cell forms as in the dry case, and there is some slight evidence of increased mass flux in the updraft due to moist convection. There is a winter jet at 1200 hPa and 60N as in the dry case, and also the remnant of a summer jet at 1200 hPa and 80S. The zonal wind pattern in the region between 1000 hPa and 200 hPa is qualitatively more similar to the moist case; a large region of easterlies dominates between two well-isolated jets. The ITCZ is further poleward than the moist ITCZ, which is causing a weakening of the summer jet and strengthening of the winter jet in the 400 hPa region. At 800 hPa, there is a region of alternating

easterlies/westerlies between the south pole and 20S; this alternating pattern exists due to the transience of the deep, precipitating updraft in the intermediate case as it progresses poleward in latitude.

Having developed an overview of the wind patterns in our simulations, we now turn to a quantitative analysis of the angular momentum budget.

3.2. Angular momentum budget

The angular momentum per unit mass is defined

$$J(u,\varphi) \;=\; (\Omega a\cos(\varphi)+u)a\cos(\varphi)\;, \tag{3}$$

where Ω is the planetary rotation rate, a is the planetary radius, u is the zonal wind velocity, and φ is the latitude. The axisymmetric primitive equations conserve angular momentum, J, in the free troposphere. In regions of surface easterlies, the surface imparts a torque on low-level air, transferring its angular momentum to the air. The Hadley circulation then lofts this air out of the viscous boundary layer, above which there are no sources or sinks of angular momentum in our axisymmetric model. In order to conserve angular momentum, meridional transport by the Hadley cell accelerates (decelerates) westerlies as air parcels move poleward (equatorward) in the free troposphere (in Equation 3, u must increase (decrease) to offset the change in $\cos(\varphi)$). The resultant angular-momentum-conserving zonal winds aloft increase approximately quadratically with latitude. The downwelling branch of the Hadley cell transports the air back to the boundary layer where angular momentum is transferred from the atmosphere to the surface in regions of surface westerlies. This qualitative picture of angular momentum transport by the Hadley cell holds when the forcing is steady; since the seasonal cycle on Titan creates an oscillating Hadley cell, the angular momentum budget may not work in the same way.

One can estimate the effect of the seasonal oscillation of the Hadley cell on the angular momentum budget by comparing the seasonal timescale to the overturning timescale. If the latter timescale is short compared to the former, the steady Hadley cell theory applies for each snapshot in time; in the opposite limit, the angular momentum is redistributed by the time-mean mass flux. An estimate of the overturning timescale comes from a ratio of the mass flux of the Hadley cell to the mass of the layer through which the mass is fluxed. The mass of this layer is

$$M \simeq A\frac{\Delta p}{g} , \tag{4}$$

where A is the surface area of Titan, Δp is the approximate change in pressure across the depth of the layer, and g is the surface gravity. The mass flux is diagnosed directly from the simulations as the maximum of the meridional streamfunction (Hadley cell). Estimates of layer masses, mass fluxes and overturning timescales for our three simulations are displayed in Table 3.

[**Table 3**]

In the moist case, the overturning timescale in long compared compared to a Titan year, while the intermediate case experiences an overturn every two Titan years (a year on Titan is 10,832 days, or 29.66 years). Inasmuch as these estimates are representative of the state at all seasons, the angular momentum in this layer is redistributed by the average mass flux. The overturn time in the dry case is comparable to a Titan year, suggesting there may be some influence of the instantaneous circulation on the angular momentum; this was evident in our description of the zonal winds in Figure 2.

The analysis based on turnover times does not take into account the episodic nature of the depth of convection, and therefore the depth of the Hadley circulation, which is particularly evident in our intermediate simulation. It also ignores time evolution of the mass flux, any secondary overturning cells that may develop, and the potentially large

solsticial mass fluxes that tend to compensate each other in the annual average. These effects can be addressed by looking at the full angular momentum budget, which we will presently address.

A more accurate approach to analyzing the effect of seasonal oscillation on the angular momentum budget can be performed by separating the momentum flux into time-mean and time-varying components. This separation is done by assuming wind velocities can be separated into constant and variable component, i.e.

$$\mathbf{v} = \mathbf{v_o} + \mathbf{v}' \tag{5}$$

where $\mathbf{v} = (u, v, w)$ are the zonal, meridional and vertical wind velocities. Quantities with the subscript $_o$ are constant and primed quantities are time-varying. It is convenient to define the mass flux

$$\mathbf{V} = 2\pi a \cos\varphi \int_{p_1}^{p_2} (v, w) \frac{dp}{g} \ . \tag{6}$$

We are interested in the meridional and vertical flux of angular momentum, which in a layer bounded by pressures p_1 and p_2 is defined

$$\mathbf{M} = 2\pi a \cos\varphi \int_{p_1}^{p_2} (v, w) J \frac{dp}{g} \ . \tag{7}$$

The time-mean, denoted by an overbar, of the angular momentum flux is found by combining Equations 3, 5, 6, and 7, whence

$$\overline{\mathbf{M}} \ = \ \overline{\mathbf{V}} \ \overline{J(u)} + \overline{\mathbf{V}' J(u')} \ . \tag{8}$$

By definition, $\overline{\mathbf{V}} \ \overline{J(u)} = \mathbf{V_o} J(u_o)$.

Figure 3 shows the meridional and vertical components of angular momentum flux integrated over the region excluding the return flow of the Hadley cell (1350-0 hPa), which we will from now on call the "free troposphere"; the solid line indicates the total time-mean angular momentum flux, the dot-dashed line is the product of the mean components of

velocity and angular momentum ("mean-product"), and the dotted line is the correlation of the time-varying components of velocity and angular momentum ("variable"). Both vertical (left column) and horizontal (right column) fluxes are shown. We have taken the average over two Titan years, which we find is a sufficient amount of time to achieve flux balance.

[**Figure 2**]

The mean-product term clearly dominates all angular momentum fluxes in the moist case; this quantitatively demonstrates our previous conclusion that since the overturning circulation is relatively slow, the angular momentum budget can be understood by transport of angular momentum by the time-mean mass flux. The time-average overturning mass flux and zonal winds for our simulations are shown in Fig. 4; warm colors indicate clockwise overturning or westerlies and cool colors indicate counter-clockwise overturning or easterlies. In the moist case, the cross-equatorial circulation at solstices (see Fig. 2) results in a symmetric, indirect circulation at low-latitudes in the time-mean, i.e. the mass flux aloft is directed up the mean temperature gradient. The Hadley cell therefore converges easterly momentum into low-latitudes, which is consistent with annual-average easterlies in this region. High-latitude jets form poleward of this region, corresponding to the time-mean direct circulation present between 40-60N/S. The inner boundary of the jets corresponds to the region of largest vertical angular momentum flux (see Fig. 3(a)); this is the region where westerly momentum is injected into the free troposphere which sustains the jets.

[**Figure 3**]

The second row of Figure 3 displays angular momentum fluxes in the intermediate case, which has several distinct features. First, the time-variable term is now contributing significantly to the angular momentum fluxes, which is as we expected from the relatively shorter overturning time. Angular momentum is primarily injected into the free troposphere near the equator and transported poleward by both the time-mean and variable compenents

of the meridional angular momentum flux. Angular momentum is returned to the surface at mid latitudes. Annual-mean zonal winds in Figure 4(d) share some similar and some unique characteristics with the moist case. The double-jet structure is robust, but significantly more hemispherically asymmetric, which is due to the asymmetry in the annual mean Hadley cell in Figure 4(c) driven by a shorter, more intense southern-hemisphere summer. Easterlies at 500 hPa are stronger than in the moist case, which by Equation 3 requires the Hadley cell updraft to have travelled further poleward during solstices (this is confirmed in Figure 6).

[**Figure 4**]

The dry case shown in the bottom row of Figure 3 is most influenced by time-variable angular momentum fluxes, again as expected from the relatively short overturning time. The annual average circulation has significantly more hemispheric asymmetry than the previous two cases. The main updraft of the Hadley cell in Figure 4(e) is displaced to the southern hemisphere; Titan's southern summer solstice is more intense due to the eccentricity of Saturn's orbit, and this causes the southern summer, cross-equatorial circulation to be the strongest of any season. Correspondingly, the latitude of angular momentum injection in Figure 3(e) is centered near 20S latitude. Meridional angular momentum fluxes spread away from this location to areas centered at 50S and 50N latitude where the angular momentum is returned to the surface by friction. During summer solstice when the Hadley cell updraft is located in the summer hemisphere, the circulation is at its strongest and the overturning time is at its shortest, and the strongest effect of the time-variable fluxes is therefore seen in mid-latitudes. The annual mean zonal winds in Figure 4(f) show relatively little hemispheric asymmetry. There is an easterly jet centered at 1200 hPa above the equator due to the equatorward convergence of angular momentum injected at 20S latitude.

A general understanding of the sensitivity of angular momentum transport to methane

vapor concentration emerges from this analysis. Under dry conditions, most of the mass flux is restricted to the layer below 1000 hPa. Due to dry-neutral conditions, the mass flux is very large which allows the circulation to respond roughly in-phase with the solar forcing; since the southern hemisphere summer is stronger than the northern, the southern time-mean Hadley cell is both more vigorous than the other cases and extends into the northern hemisphere. In the annual average, the upper branch of the Hadley cell brings easterly momentum to low latitudes and produces and sustains easterlies at the top of the Hadley cell. In moist conditions, deep convection allows transport of angular momentum deeper into the free troposphere by the Hadley circulation. Two indirect cells span low- to mid-latitudes, which converge easterly momentum into low latitudes aloft. Direct cells poleward of this region create and sustain jets at high-latitudes. The intermediate case is a hybrid of the moist and dry cases. In the absence of precipitation, the Hadley cell is shallow and intense as in the dry case, and at solstices when precipitation is present, the Hadley cell is deep as in the moist case. The episodic, deep convection at solstices sustains more intense easterlies at 500 hPa than in the moist case because the ITCZ migrates further poleward at solstices.

Since Huygens observed low-latitude westerlies above 1000 hPa and easterlies below, there seems to be a paradox emerging. Observed mid- and high-latitude convective clouds suggest Titan's Hadley cell oscillates, as is born-out in our simulations. But the annual-average circulation results in low-latitude easterlies, contrary to the Huygens observation. Our calculations suggest horizontal eddy transport (or some other source) of angular momentum is necessary to produce low-latitude westerlies where Huygens observed them. Axisymmetric simulations by *Rannou et al.* (2006) do produce low-latitude westerlies, which are the result of parameterized mixing of linear momentum. A complete understanding of the angular momentum budget in simulations consistent with observations of Titan's methane cycle is lacking, and will require a detailed study of the three-dimensional

dynamics.

Barotropic eddies that can mix angular momentum up the zonal-mean gradient are known to likely produce and sustain superrotating winds in the stratosphere (*Hourdin et al.* 1995), and perhaps this is the mechanism responsible for low-latitude westerlies in the troposphere. A necessary condition for barotropic instability is that the meridional gradient of the potential vorticity, q_y, change sign in the interior.

In latitudes with jets, q_y of the zonal-mean flow is primarily the result of horizontal shear in the zonal winds; on a β-plane the absolute vorticity gradient is estimated

$$q_y \simeq \beta - u_{yy} , \tag{9}$$

where $\beta = 2\Omega\cos(\varphi_o)/a$ is the meridional gradient of planetary vorticity at latitude φ_o (which we roughly take to be the latitude of the jet) and u_{yy} is the curvature of the mean flow (*Vallis* 2006).[3] In other words, narrow jets have large vorticity gradients on their flanks and can be a source of energy conversion from zonal flow to barotropic eddies. Figure 5 shows q_y (shaded contours) and zonal winds (lines) of the northern-hemisphere jet as lines at SSS in our moist simulation; warm(cool) colors indicate positive(negative) q_y. The jet appears to be barotropically unstable, since q_y changes sign on its flanks. In a three-dimensional model, this configuration could produce barotropic eddies that mix the angular momentum of the jets up gradient to produce low-latitude westerlies. 3D simulations are required to assess whether this mechanism is sufficient to produce low-latitude westerlies at 10 m/s in the troposphere (see e.g. *Williams* (2003)).

---

[3]The absolute vorticity is used as a proxy for potential vorticity; the latter quantity includes the contribution of "column stretching". The β-plane approximation is valid for a narrow region in latitude around φ_o, in which $f \simeq f_o + \beta\varphi a$, where f_o is the planetary vorticity evaluated at φ_o.

[Figure 5]

3.3. Consistency with Observations

Here we compare our model simulations with the available data. We focus particular attention on precipitation/cloud patterns, temperatures, winds, and methane concentrations.

3.3.1. Precipitation and convection

In *Mitchell et al.* (2006), we presented the precipitation patterns predicted by our three scenarios and compared them to cloud observations. Here we summarize the same analysis for our cases with shortwave absorption included. Figures 6(a),(c),(e) show contour plots of precipitation for our three dynamical simulations over one Titan season with solar forcing at the surface overlaid for reference. We infer clouds in our simulations by the presence of moist convection, which always produces precipitation in our convection scheme. Figures 6(b),(d),(f) show the annual mean convective drying in g/kg/day in order to highlight where the production of clouds would be favorable.

[Figure 6]

The dry case, in which we have removed the latent heating of methane, generally lacks the isolation of convection necessary to reproduce the observed clouds. The Hadley cell updraft spans the summer hemisphere during solstices, allowing convection to occur at all summer latitudes. In the dry limit, methane is advected by the dynamics and condenses in the atmosphere to produce precipitation without affecting the thermal structure. The dry case should not be thought of as representing an actual planet, but by comparison to moist

simulations serves to illustrate the effect of methane thermodynamics on the circulation of the atmosphere. The Hadley cell switches direction with season and is in-phase with the solar forcing. Convection is generally shallower than the observed cloud heights, as would be expected in the absence of latent heat release.

The moist case, in which the latent heat of methane condensation/evaporation is included, shows evidence of the control of moisture on the large-scale circulation. The ITCZ, marked by a band of narrow precipitation, is narrowed and enhanced in strength relative to the dry case. Dry air descends over the rest of the globe and surface air diverges methane towards the updraft; the combination of these effects suppresses moist convection outside of the ITCZ. The ITCZ is out-of-phase with solar forcing and only reaches 60N/S latitude, a characteristic to which we will return in Section 3.4.1. Narrow streaks of precipitation emanate from the equator toward the solsticial pole. These features, which in *Mitchell et al.* (2006) were more evident in the intermediate case, are due to symmetric instabilities; their origin and evolution will be the subject of future work. The solsticial polar regions experience poorly organized precipation that is more in-phase with the solar forcing than the ITCZ. The polar regions experience very weak precipitation throughout the year. Convection extends deep into the atmosphere, reaching altitudes consistent with observed convective clouds (*Griffith et al.* 2005). The location of precipitating convection is consistent with observed cloud locations, though the moist case tends to overproduce convection at summer mid-latitudes relative to the summer pole.

The intermediate case includes the latent heat of methane condensation/evaporation, but methane is kept sub-saturated by surface evaporation in the absence of large-scale convergence and/or radiative cooling. The model produces an isolated ITCZ as in the moist case which travels pole-to-pole with the progression of the seasons. However, precipitation only occurs episodically near solstices and only in the summer hemisphere. The atmosphere

is slightly less out-of-phase with solar forcing than in the moist case, though some phase lag is evident. A few intense, isolated precipitation events occur directly at the summer poles. Convective drying rates are isolated in latitude, as seen in Figure 6(f). Latitudes near 75S experience the most precipitation. The presence of well-isolated convection only in the summer hemisphere makes the intermediate case consistent with cloud observations. As in the moist case, however, the model tends to overproduce precipitation at high summer latitudes relative to the summer pole.

Dunes are observed to be prevalent in the equatorial regions bounded by 30 N/S latitude (*Lorenz and Radebaugh* 2009), suggesting climatologically dry conditions prevail there. Our model results are not inconsistent with this observation since the equatorial regions experience net drying in cases with the latent heat of methane included. This topic is covered in detail in a companion paper (*Mitchell* 2008). A perhaps related phenomenon is the presence of hydrocarbon lakes located solely in polar regions (*Stofan et al.* 2007). The transport of methane away from low latitudes towards high latitudes by the large-scale circulation may account for the grouping of lakes near the poles. "Ponding" in dry lake beds is also observed to occur rather quickly, presumably following large convective storms at the summer pole (*Turtle et al.* 2009). While our analysis is not aimed at characterizing the synoptic meteorology of methane storms, bursts of convective activity at the summer poles is evident in Figures 6(c) and (e), which may account for this ponding. An accounting of surface methane hydrology is needed for comparison with these observations, and we explore this in *Mitchell* (2008).

3.3.2. Temperatures

At the Huygens location and epoch, 10S latitude and just following southern summer solstice, the lowest few km are on the dry adiabat, and dry-stable radiative equilibrium

sets the temperature profile above. Figure 7 shows the Huygens (red) temperature profile as compared with our simulations at 10S latitude during the Huygens epoch (solid black – moist case; dot-dashed – intermediate case; dashed – dry case; blue line – radiative equilibrium of our model). The moist case (solid black line) experiences deep, precipitating convection, and temperatures follow the moist adiabat up to 30 km altitude. The dry case (dashed line) is subject to dry convection in the lowest 15 km of the atmosphere, and the layers above are close to radiative equilibrium. The dry case overestimates the surface temperature and depth of the dry convective layer; the latter results from the approximations of the "dry limit" of our moist convection scheme (see description at the beginning of Section 3). Temperatures in the intermediate case (dashed line) are on the dry adiabat up to 5 km, then follow the moist adiabat from 5-30 km, signaling that deep, precipitating convection influences the thermal structure of this layer. The intermediate case is somewhat biased towards more frequent convection since we have lowered the convective threshold to 40% relative humidity, an assumption which is enforced to more steadily release CAPE.[4]

[**Figure 7**]

Table 4 shows the maximum surface temperature difference between 60S and 60N latitude at northern spring equinox for our simulations as well as two radiative-convective cases compared to that inferred from Voyager observations (*Samuelson et al.* 1997). Our dynamical simulations reproduce the observed weak equator-to-pole surface temperature gradient of a few Kelvin. Radiative-convective (labeled "R-C") simulations, in contrast, show a much larger surface temperature gradient of between $20 - 40K$, so the global

[4] *Frierson* (2007) shows the ability to build up and release CAPE is a key distinguishing characteristic of convection schemes. The interested reader is referred to this reference for further discussion.

Hadley cell is strongly reorganizing the thermal structure in the troposphere, as expected from tropical dynamics theory (*Held and Hou* 1980). The intermediate case is again most consistent with the observations.

[**Table 4**]

3.3.3. Winds

The Doppler Wind Experiment on the Huygens probe, which descended at around 10^oS latitude, measured easterlies in the lowest 8-10 km and weak westerlies with positive shear (increasing westerlies with hight) above (*Bird et al.* 2005). As discussed in Section 3.2, the strong, solsticial ITCZ of the oscillating Hadley cell injects low-angular-momentum air from the high-latitude surface into the free troposphere; easterlies form at latitudes equatorward of the ITCZ as low-angular-momentum air parcels are displaced to lower latitudes by the large-scale circulation. By this mechanism, all three cases produce westerly jets at high latitudes. In all cases, the circulation carries low angular momentum from the polar, solsticial ITCZ equatorward, which sustains easterlies at nearly all latitudes except for the location of the jets. None of our cases produce low-latitude westerly winds above 10 km at the Huygens epoch.

There are a few possible reasons for this discrepancy with observations. First, as noted earlier, simulations by *Hourdin et al.* (1995) show barotropic eddies mix momentum from westerly jets up-gradient and produce super-rotation in the stratosphere. This mechanism could also operate in the upper troposphere to produce the observed low-latitude westerlies. It is left to future work to explore this mechanism in a three-dimensional model. Second, since Titan's rotation rate is relatively low, the gradient wind relation implies small changes in the latitudinal temperature gradient can result in large changes in the zonal winds.

It is difficult to say whether local temperature gradients can become extreme enough to affect the zonal wind pattern, but it should be kept in mind as more observations become available.

RADAR observations of dunes near the equator suggest a surface wind pattern that is oriented in the prograde direction (*Lorenz and Radebaugh* 2009). This wind pattern is very difficult to explain in the context of frictional angular momentum coupling between the surface and atmosphere; the equatorial surface has the largest angular momentum of any latitude, and one expects air in frictional contact with this region not to exceed solid-body rotation. This phenomenon almost certainly involves 3D momentum transport, and is therefore beyond the scope of our simplified model atmosphere.

The profile of vertical winds was also inferred from the Huygens descent data (*Mäkinen et al.* 2006). A weak updraft persists through the lowest 8 km, capped by several layers of updrafts separated by narrow downdrafts. The moist simulation has low-latitude downdrafts at the Huygens epoch, which is inconsistent with the Huygens observation. The dry and intermediate cases have updrafts near the surface at low latitudes. The intermediate case also has layered up/downdrafts above 8 km altitude as is evident in Fig. 4(c). We therefore conclude the intermediate case is most consistent with the observed vertical wind.

3.3.4. Methane vapor profile

The Huygens probe measured the abundance of methane during its descent (*Niemann et al.* 2005). The vertical profile of methane approximately follows saturation at the ambient temperatures until an altitude of 8 km. Below, the mole fraction of methane is constant, temperatures are on the dry adiabat, and therefore the relative humidity drops from close to saturation at 8 km to ∼45% at the surface. Our intermediate simulation produces

this type of profile. Dry convection and the resulting circulation homogenize the methane vapor through the lowest 8 km in a manner similar to that seen in simulations with more realistic methane hydrology in *Mitchell* (2008). In regions of large-scale convergence of surface-level air, parcels are lifted above 8 km and trigger moist convection. The moist case is inconsistent with the observations since the surface-layer air is being efficiently moistened to near saturation; in this case, the methane mole fraction increases monotonically to the surface since moist convection efficiently redistributes methane in the column. By construction, therefore, the intermediate case produces a methane profile that is most similar to the observations. Despite being the standard modeling approach in moist Titan GCMs (*Tokano et al.* 2001; *Rannou et al.* 2006; *Mitchell et al.* 2006), there is no physical justification for reducing the relative humidity of the surface-level air.

3.4. Analysis

Having described the simulations in detail, we now perform further diagnostic analysis in three areas. In Section 3.4.1, we establish a physical understanding of the varying thermal inertia across our simulations. In Section 3.4.2, we examine energy transport by our model atmosphere.

3.4.1. Thermal inertia of Titan's climate system

The varying amount of phase lag of the ITCZ in our simulations suggests the thermal inertia of the climate system changes with varying methane vapor concentrations. In the previous section, we suggested this has to do with the amount of coupling between the low-thermal-inertia surface and high-therma-inertia atmosphere by convection. Solar energy is deposited in the surface and then communicated into the atmosphere by convection;

temperatures are horizontally homogenized in the Hadley domain. Once warmed by convection, air parcels cool radiatively on a timescale that is long compared to a Titan season; this radiative timescale gives a measure of the thermal inertia. Therefore the depth of the convective layer should be correlated with the amount of thermal inertia in the climate system. Methane mediates heat transfer between the surface and atmosphere since moist convection penetrates more deeply into the atmosphere than dry convection and therefore warms a greater mass of the high-heat-capacity atmosphere. In the Introduction, we discussed the radiative cooling timescale for the entire depth of Titan's optically thick atmosphere (heat capacity per unit area $C = c_p p_s/g$). But the depth of the convective layer, p_{conv}, can be significantly smaller than the entirety of the atmosphere, which effectively reduces the heat capacity ($C = c_p(p_s - p_{conv})/g$), and therefore thermal inertia, of the system.

To gain intuition on the effect of thermal inertia on the response of the climate to seasonal forcing, we turn to a "box" model intended to represent a large-scale average of the atmosphere-surface system. The box model assumes the atmosphere and surface combine into one reservoir of thermal inertia that is forced by a varying source representative of the seasonal cycle of insolation. The box has a single prognostic variable, the temperature perturbation T' about the mean T_o, a parameter representing the thermal inertia τ_{in}, and a specified, sinusoidally varying source term with period $P = 2\pi/\omega$, which corresponds to the length of a full seasonal cycle. The temperature perturbation of the box follows the prognostic equation,

$$\frac{dT'}{dt} = -\frac{T'}{\tau_{in}} + \frac{\overline{T}}{\tau_f} e^{i\omega t} , \tag{10}$$

where τ_{in} is the thermal inertia of the system and τ_f is the timescale of the forcing toward $\overline{T}$. As a simplifying assumption, we will take $\tau_{in} = \tau_f$. The first term on the RHS tends to damp temperatures towards T_o, and can be thought of as the radiative cooling of the system. The second term on the RHS represents the seasonal oscillation of the solar forcing

which warms the atmosphere-surface system both directly by shortwave absorption and indirectly by convection. Equation 10 has the solution

$$T = T_o + \overline{T}\frac{e^{i\omega t}}{i\omega\tau_{in} + 1} \tag{11}$$

We will explore limits of this system to develop our intuition.

$\omega\tau_{in} << 1$:
This limit occurs when the thermal inertia is much shorter than the seasonal period. Temperature perturbations about the mean are in-phase with the forcing term and respond to the full forcing amplitude.

$\omega\tau_{in} >> 1$:
This limit occurs when the thermal inertia of the system greatly exceeds the seasonal period. In this limit, Equation 11 reduces to $T = T_o - i\ \overline{T}e^{i\omega t}(\omega\tau_{in})^{-1}$. The amplitudes of perturbations to the mean temperature are reduced relative to the forcing by a factor of $(\omega\tau_{in})^{-1}$ and the phase lags the forcing term by 90^o (1/4 period).

$\omega\tau_{in} = 1$:
If the thermal inertia has the same magnitude as the seasonal period, Equation 11 reduces to $T = T_o + (1 - i)\ \overline{T}e^{i\omega t}/2$. Temperature perturbations are reduced in amplitude by a factor of two and have a phase lag of 45^o (1/8 period) relative to the forcing term.

The plots of seasonal precipitation patterns, Fig. 6, give an estimate of the phase-lag between the solar forcing and the response of the circulation, which are shown in the middle column of Table 5. The lowest phase lag is apparent in the dry case. If the dry case corresponds to the box model in the limit $\omega\tau_{in} << 1$, we also expect the amplitude of temperature changes to be greatest in the dry case. Figure 8 shows the amplitude of temperature changes over one Titan year as a function of latitude and height in our three simulations; the amplitude is diagnosed as the maximum temperature minus the

minimum temperature for each grid box during one season and estimates are given in the rightmost column of Table 5. It is indeed the case that the amplitude of the temperature response to seasonal forcing is greatest in the dry case, almost twice as much as the greatest temperature change in the other two cases. The amplitude of temperature changes in the moist and intermediate cases are similarly smaller in magnitude than the dry case, which suggests higher levels of thermal inertia in these systems relative to the dry case. This effect is also seen in the phase lags of the ITCZs of these simulations. In the moist case, Fig. 6 shows the ITCZ only oscillates between 70N and 70S, and in this region the amplitudes of temperature oscillations in Fig. 8(a) are lower than in any other case. Poleward of this region, where the precipitation responds in-phase with the solar forcing, amplitudes are similar to the intermediate case. These features suggest the moist and intermediate cases are closer to the limit of large thermal inertia, $\omega\tau_{in} > 1$, particularly in the moist case where the ITCZ is nearly in quadrature (phase lag near 90^o or 7 years) with the seasonal forcing.

[**Figure 8**]

[**Table 5**]

The seasonal responses of our simulations can be summarized as follows. The dry case shows the least amount of thermal inertia as measured both by the negligible phase lag of the ITCZ with solar forcing and by large amplitude seasonal temperature perturbations. The intermediate case shows lower amplitude in temperature extrema and a small amount of phase lag, which both indicate more thermal inertia than the dry case. Compared with the intermediate case, the moist case shows smaller amplitude in temperature extrema and an ITCZ nearly in quadrature with solar forcing, signaling the greatest amount of thermal inertia.

The amount of thermal inertia in our simulations can be attributed to the depth of convection and the persistence of the deep convection. In the absence of methane

condensation, shallow (dry) convection probes relatively little atmospheric mass, which results in no phase lag and high amplitude temperature extrema in the dry case. Persistent deep convection in the moist case significantly increases the amount of atmospheric mass warmed by convection, and therefore increases thermal inertia of the system; as a result, the ITCZ responds nearly in quadrature with the seasonal forcing and produces the weakest seasonal temperature changes of the three simulations. Sporadically deep convection in the intermediate case results in intermediate phase lag and intermediate-amplitude temperature extrema. All of these features are consistent with the intuition of thermal inertia developed from the box model, Equation 11.

3.4.2. Energy and mass fluxes

Energy is transported in the atmosphere by the advection of dry static energy (DSE) and the latent heat of moisture (M). The meridional energy fluxes associated with DSE and M are defined

$$M(\varphi) = 2\pi a \cos(\varphi) \frac{L_v}{g} \int_{p_s}^{0} vq \; dp \tag{12}$$

$$DSE(\varphi) = 2\pi a \cos(\varphi) \frac{1}{g} \int_{p_s}^{0} v(C_p T + gz) \; dp \tag{13}$$

where a is the radius of Titan, L_v is the latent heat of vaporization for methane, C_p is the heat capacity of air, g is Titan's surface gravity, v is the meridional velocity, q is the mass mixing ratio of methane (in Kg/Kg), T is the temperature, z is the height, and p is the atmospheric pressure. The sum of the two fluxes is referred to as the moist static energy (MSE) flux. Since the annual-mean insolation maximum is at the equator, the annual-mean Hadley cell must transport heat away from this region in order to make temperatures uniform; we will refer to this as the "angular momentum constraint" since the thermal wind relation and angular momentum conservation requires flat temperature gradients near the

equator where the coriolis effect vanishes (see *Held and Hou* (1980)). This heat transport can be accomplished by the flux of dry static energy or by moisture flux, however, and these do not, in general, act in the same direction.

Figure 9 shows annual-mean energy fluxes in our three simulations; the black lines indicate MSE fluxes, dotted lines indicate DSE fluxes, and dot-dashed lines indicate moisture fluxes (the dry case only has DSE flux). Positive (negative) fluxes indicate net northward (southward) flux of energy. As expected from the angular momentum constraint, the total energy flux diverges at low-latitudes and has roughly the same magnitude in all cases.

[**Figure 9**]

In both the moist and intermediate cases, moisture is fluxed away from equatorial regions by the seasonally oscillating Hadley cell. In the moist case, DSE fluxes are negligible in the region of net moisture divergence while poleward of this region the moisture fluxes are negligible and DSE fluxes contribute the bulk of the energy transport. The latitude at which this changeover occurs is at the the maximum latitudinal excursion of the precipitating ITCZ in Figure 6(c). In the intermediate case, moisture is diverged away from a slightly wider band of latitudes than in the moist case; the sensitivity of low-latitude moisture divergence to model parameters and its implication for the presence of equatorial deserts is discussed in *Mitchell* (2008). Energy fluxes in the intermediate case have noticeably more hemispheric asymmetry than the moist case; DSE fluxes contribute significantly to northward energy transport, but not to southward transport.

The thermally indirect orientation of the low-latitude annual-mean mass flux in our moist simulation (Figure 4(a)) and the hemispheric asymmetry in the intermediate case (Figure 4(c)) create a unique regime of energy transport: moisture is fluxed away from the equator. This is opposite to the case on Earth, where the annual-mean Hadley cells

are thermally direct and converge moisture onto the equator. In both climates, moisture is converged to the annual-mean updraft. The difference can be understood from the fact that Titan's annual-mean updraft is at mid or high latitudes while Earth's is at the equator. Low-latitude moisture divergence has significant implications for the surface moisture budget, which is discussed in detail in *Mitchell* (2008). A discussion of the effects of moisture on MSE fluxes in the context of altered Earth-like climates can be found in *Frierson et al.* (2007).

The observed convective clouds at summer mid and high latitudes (e.g. *Porco et al.* (2005), *Roe et al.* (2005)), recent evidence for low-latitude deserts (*Lorenz et al.* 2006) and high-latitude lakes (*Stofan et al.* 2007) on Titan, and relatively dry near-surface air at the Huygens landing site (*Niemann et al.* 2005) all suggest the climatology of precipitation and surface morphologies are correlated. In either the intermediate or moist cases, net drying occurs at low-latitudes, and therefore these cases are consistent with observed low-latitude deserts. *Perron et al.* (2006) show the observed fluvial features imbedded in Titan's dunes require episodes of methane rain with 0.5-15 mm/hr precipitation rates at low latitudes. This is consistent with our modeling results since the moist case produces precipitation near the equator (Figure 6(c)); the climatological classification of the low latitudes as deserts does not necessarily rule out seasonal episodes of low-latitude precipitation. The observation that deserts probably cover around half of the surface of Titan (roughly half of the area of a sphere is within $\pm 30^o$) suggests the assumption of an infinite surface reservoir of liquid methane is invalid for Titan. A model with a limited reservoir of methane is needed to self-consistently study the connection between surface morphology and climate, and we expore this connection in a companion paper (*Mitchell* 2008).

4. Conclusions

We have modeled the seasonal behavior of Titan's troposphere in a variety of methane hydrology scenarios using a novel convection scheme in an axisymmetric atmospheric model. We presented three simulations of Titan spanning the range from "moist" to "dry", i.e. with and without methane thermodynamics included. In the "moist" case we allowed the surface to efficiently moisten the boundary layer toward saturation, in the "intermediate" case we limited the boundary layer moistening to 50% relative humidity (as has been done in other studies (*Tokano et al.* 2001; *Rannou et al.* 2006)), and in the "dry" case we removed the latent heat of methane entirely while allowing evaporation and condensation to occur. We then systematically compared model diagnostics to observations where available.

In the moist and intermediate cases the ITCZ is enhanced and narrowed compared to the dry case due to the release of latent heat. Methane is globally converged to the updraft of the Hadley cell at the surface, and broad regions of large-scale subsidence suppress convection over much of the globe. Two areas of moist convection develop at solstices in the moist case, one well-organized ITCZ at mid summer latitudes and an area of more diffuse precipitation near the summer pole. The locations of these features are consistent with the observed convective clouds, though the model produces more persistent convection than is observed at mid latitudes. The intermediate case has a single moist convective ITCZ which reaches to higher summer latitudes and very episodic polar convective events.

The intermediate case is most consistent with the Huygens profiles of temperature and humidity. Model methane relative humidities at the Huygens location and epoch decrease from near saturation at 8 km to ∼45% at the surface, and the mole fraction is nearly constant in this altitude range. Model temperatures are on the dry adiabat between the surface and 8 km (1500-1000 hPa) and close to radiative equilibrium above 8 km, as observed. In contrast, persistent, deep convection constrains model temperatures to the

moist adiabat through much of the column in the moist case, and the dry case overestimates the depth of the dry convective layer.

The thermal inertia evident in the form of phase lag of the ITCZ with seasonal insolation and amplitude of seasonal temperature changes can be understood by the coupling of the low-heat-capacity surface and high-heat-capacity atmosphere by convection. In the moist case, an unrestricted surface methane supply allows persistent deep convection, which warms a large fraction of the mass of the atmosphere. The ITCZ in the moist case is nearly in quadrature with the insolation pattern and has the lowest seasonal temperature changes, both of which signify a large thermal inertia. In the dry case, the lack of methane moisture restricts the depth of convection to a shallow layer; the ITCZ in this case is in-phase with solar forcing and the atmosphere has large temperature changes with season, and therefore has the least thermal inertia of the three cases. A restricted supply of surface methane in the intermediate case only allows sporadic deep convection. The intermediate case has intermediate levels of phase-lag and temperature changes, and we therefore infer an intermediate amount of thermal inertia.

Strong seasonal oscillations of the Hadley cell create a thermally indirect annual-mean mass flux at low latitudes in the moist case, with updrafts at mid or high latitudes and downdrafts at the equator. In the moist and intermediate cases, the indirect mass flux diverges moisture out of low latitudes which is the opposite sense in which they are directed on Earth. In the dry case, the circulation accomplishes poleward transport of dry static energy as required by the angular momentum constraint.

High- latitude and altitude zonal winds exceed 20 m/s in all cases. None of our cases produce low-latitude westerlies observed at the Huygens epoch (*Bird et al.* 2005); one must appeal to non-axisymmetric processes in order to produce low-latitude westerlies. The intermediate case produces alternating up/down-drafts at low latitudes as symmetric eddies

formed at the equator move toward the solsticial pole and grow. The dry and intermediate cases produce updrafts in the lowest few kilometers at the Huygens epoch, as observed (*Mäkinen et al.* 2006), while the moist case does not.

Observed surface morphologies, particularly low-latitude deserts (*Lorenz et al.* 2006), are climatologically consistent with the moist and intermediate cases. Net, annual-mean drying within $\pm 40^o$ latitude occurs in these cases, yet low-latitude, seasonal precipitation can occur and have the potential to create the observed fluvial features imbedded in Titan's dunes (*Perron et al.* 2006). The lack of a global ocean on Titan suggests a model accounting for the surface redistribution of methane is needed to self-consistently explore the link between climate and surface morphology. The feedback between surface supply of methane and the seasonal response of the circulation further corroborates this need. The sensitivity of the climate to the size of the methane reservoir is explored in a companion paper by coupling a simple, terrestrial "soil model" to our model atmosphere (*Mitchell* 2008).

A potential paradox emerges from these simulations. Our results indicate that while the intermediate case is most consistent with the observed thermodynamic state, surface climatological zones, and cloud distributions, it is inconsistent with observed low-latitude westerlies. The oscillating Hadley cell produces strong cross-equatorial flow during solstices which transports low-angular-momentum air parcels to low latitudes and sustains low-latitude easterly zonal flow. Even if the Hadley circulation were somehow steady and equatorially symmetric, low-latitude westerlies at 10 m/s can only occur in the presence of momentum mixing by three-dimensional eddies. High-latitude westerly jets are produced at 20 m/s which are barotropically unstable and could therefore source eddies that mix momentum back toward low latitudes. A full accounting of angular momentum requires the addition of a parameterization of horizontal momentum mixing to the two-dimensional model or three-dimensional simulations that self-consistently produce eddies. We plan to

explore both of these scenarios in future work.

Our simulations employ idealized physical parameterizations for convection and radiation and ignore non-axisymmetric fluid motions. While the broad consistency of our results with observations is encouraging, more work is required to address the limitations of our approach. Areas that could be improved include, but are not limited to, the inclusion of 3D wave transports, wavelength-dependent radiative transfer, vapor-liquid equilibrium effects on methane condensation in the presence of nitrogen, and choice of convective parameterization. Such additions would necessarily add to the complexity of the model and potentially confuse interpretation of the results. In the future when more realistic models become routine, idealized models such as the one presented here could then be used to help illuminate the physical mechanisms connecting observations and modeling.

REFERENCES

Barth, E. L., and S. C. R. Rafkin (2007), Trams: A new dynamic cloud model for titan's methane clouds, *Geophysical Research Letters*, *34*(3), L03,203.

Bird, M. K., et al. (2005), The vertical profile of winds on titan, *Nature*, *438*(7069), 800–802.

Bouchez, A. H., and M. E. Brown (2005), Statistics of Titan's South Polar Tropospheric Clouds, *ApJ*, *618*, L53–L56, doi:10.1086/427693.

Brown, M. E., A. H. Bouchez, and C. A. Griffith (2002), Direct detection of variable tropospheric clouds near Titan's south pole, *Nature*, *420*, 795–797.

Caballero, R., R. T. Pierrehumbert, and J. L. Mitchell (2008), Axisymmetric, nearly-inviscid circulations in non-condensing radiative-convective atmospheres, submitted to Quarterly Journal of the Royal Meteorological Society.

Flasar, F. M., R. E. Samuelson, and B. J. Conrath, B. J. (1981), Titan's atmosphere - temperature and dynamics, *Nature*, *292*(5825), 693–698.

Frierson, D. M. W. (2007), The dynamics of idealized convection schemes and their effect on the zonally averaged tropical circulation, *Journal of the Atmospheric Sciences*, *64*(6), 1959–1976.

Frierson, D. M. W., I. M. Held, and P. Zurita-Gotor (2006), A gray-radiation aquaplanet moist gcm. part i: Static stability and eddy scale, *Journal of the Atmospheric Sciences*, *63*(10), 2548–2566.

Frierson, D. M. W., I. M. Held, and P. Zurita-Gotor (2007), A Gray-Radiation Aquaplanet Moist GCM. Part II: Energy Transports in Altered Climates, *Journal of Atmospheric Sciences*, *64*, 1680–+, doi:10.1175/JAS3913.1.

Griffith, C. A., et al. (2005), The Evolution of Titan's Mid-Latitude Clouds, *Science*, *310*, 474–477, doi:10.1126/science.1117702.

Held, I. M., and A. Y. Hou (1980), Non-linear axially-symmetric circulations in a nearly inviscid atmosphere, *Journal of the Atmospheric Sciences*, *37*(3), 515–533.

Hirtzig, M., A. Coustenis, E. Gendron, P. Drossart, M. Hartung, A. Negrao, P. Rannou, and M. Combes (2007), Titan: Atmospheric and surface features as observed with nasmyth adaptive optics system near-infrared imager and spectrograph at the time of the huygens mission, *Journal of Geophysical Research-Planets*, *112*(E2), E02S91.

Hirtzig, M., et al. (2006), Monitoring atmospheric phenomena on titan, *Astronomy & Astrophysics*, *456*(2), 761–774.

Hourdin, F., O. Talagrand, R. Sadourny, R. Courtin, D. Gautier, and C. P. McKay (1995), Numerical-simulation of the general-circulation of the atmosphere of titan, *Icarus*, *117*(2), 358–374.

Hueso, R., and A. Sanchez-Lavega (2006), Methane storms on saturn's moon titan, *Nature*, *442*(7101), 428–431.

Lorenz, R. D., and J. Radebaugh (2009), Global pattern of Titan's dunes: Radar survey from the Cassini prime mission, *Geophys. Res. Lett.*, *36*, 3202–+, doi:10.1029/2008GL036850.

Lorenz, R. D., et al. (2006), The sand seas of titan: Cassini radar observations of longitudinal dunes, *Science*, *312*(5774), 724–727.

Lorenz, R. D., et al. (2008), Titan's inventory of organic surface materials, *Geophys. Res. Lett.*, *35*, 2206–+, doi:10.1029/2007GL032118.

Mäkinen, J. T. T., A. M. Harri, T. Tokano, H. Savijärvi, T. Siili, and F. Ferri (2006), Vertical atmospheric flow on titan as measured by the hasi instrument on board the huygens probe, *Geophysical Research Letters*, *33*(21), L21,803.

Mitchell, J. L. (2008), The drying of Titan's dunes: Titan's methane hydrology and its impact on atmospheric circulation, *Journal of Geophysical Research (Planets)*, *113*, 8015–+, doi:10.1029/2007JE003017.

Mitchell, J. L., R. T. Pierrehumbert, D. M. W. Frierson, and R. Caballero (2006), The dynamics behind titan's methane clouds, *PNAS*, *103*(49), 18,421–18,426.

Niemann, H. B., et al. (2005), The abundances of constituents of titan's atmosphere from the gcms instrument on the huygens probe, *Nature*, *438*(7069), 779–784.

Perron, J. T., M. P. Lamb, C. D. Koven, I. Y. Fung, E. Yager, and M. Ádámkovics (2006), Valley formation and methane precipitation rates on Titan, *Journal of Geophysical Research (Planets)*, *111*, 11,001–+, doi:10.1029/2005JE002602.

Porco, C. C., et al. (2005), Imaging of Titan from the Cassini spacecraft, *Nature*, *434*, 159–168, doi:10.1038/nature03436.

Rannou, P., F. Montmessin, F. Hourdin, and S. Lebonnois (2006), The latitudinal distribution of clouds on titan, *Science*, *311*(5758), 201–205.

Roe, H. G., A. H. Bouchez, C. A. Trujillo, E. L. Schaller, and M. E. Brown (2005), Discovery of Temperate Latitude Clouds on Titan, *ApJ*, *618*, L49–L52, doi:10.1086/427499.

Samuelson, R. E., N. R. Nath, and A. Borysow (1997), Gaseous abundances and methane supersaturation in titan's troposphere, *Planetary and Space Science*, *45*(8), 959–980.

Schaller, E. L., M. E. Brown, H. G. Roe, and A. H. Bouchez (2006a), A large cloud outburst at Titan's south pole, *Icarus*, *182*, 224–229, doi:10.1016/j.icarus.2005.12.021.

Schaller, E. L., M. E. Brown, H. G. Roe, A. H. Bouchez, and C. A. Trujillo (2006b), Dissipation of Titan's south polar clouds, *Icarus*, *184*, 517–523, doi: 10.1016/j.icarus.2006.05.025.

Stofan, E. R., et al. (2007), The lakes of titan, *Nature*, *445*(7123), 61–64.

Thompson, W. R., J. A. Zollweg, and D. H. Gabis (1992), Vapor-liquid-equilibrium thermodynamics of n2 + ch4 - model and titan applications, *Icarus*, *97*(2), 187–199.

Tokano, T. (2005), Meteorological assessment of the surface temperatures on titan: constraints on the surface type, *Icarus*, *173*(1), 222–242.

Tokano, T., F. M. Neubauer, M. Laube, and C. P. McKay (2001), Three-dimensional modeling of the tropospheric methane cycle on titan, *Icarus*, *153*(1), 130–147.

Turtle, E. P., J. E. Perry, A. S. McEwen, A. D. DelGenio, J. Barbara, R. A. West, D. D. Dawson, and C. C. Porco (2009), Cassini imaging of Titan's high-latitude lakes, clouds, and south-polar surface changes, *Geophys. Res. Lett.*, *36*, 2204–+, doi:10.1029/2008GL036186.

Vallis, G. K. (2006), *Atmospheric and Oceanic Fluid Dynamics*, Atmospheric and Oceanic Fluid Dynamics, by Geoffrey K. Vallis, pp. 770. Cambridge University Press, November 2006. ISBN-10: 0521849691. ISBN-13: 9780521849692, doi: 10.2277/0521849691.

Williams, G. P. (2003), Barotropic Instability and Equatorial Superrotation., *Journal of Atmospheric Sciences*, *60*, 2136–2152, doi:10.1175/1520-0469(2003)060.

Table 1: A summary of model parameters, including orbital parameters for Saturn used to calculate seasonal solar forcing. See text for definitions.

Description	Parameter	Value
Planetary radius	a	2575 km
Surface gravity	g	1.35 m/s^2
Surface pressure	p_s	1.5x10^5 Pa
Rotation rate	Ω	4.5x10^{-6} s^{-1}
IR optical depth	τ_∞	10
Surface heat capacity	C	2x10^5 J/m^2/K
Surface roughness	C_d	1.3x10^{-3}
Gustiness parameter	U	5 m/s
Density e-folding	ρ_e	0.01 kg/m^3
Latent heat of vaporisation	L_v	5.1x10^5 J/kg
Convective relative humidity	rh_{BM}	0.4-0.8
Convective timescale	τ_{BM}	7200 s
Boundary layer relative humidity	rh_s	0.5-1
Vertical diffusivity	ν	10^{-2} m^2/s
Boundary layer depth		1.5-1.25x10^5 pa
Orbital eccentricity (Saturn)		0.054
Orbital semi-major axis (Saturn)		9.5 AU
Longitude of ascending node (Saturn)		100 degrees

Table 2: Parameters differing between our three modeling cases.

Case	L_v	rh_s	rh_{BM}
Moist	5.1x10^5 J/kg	1	0.8
Intermediate	5.1x10^5 J/kg	0.5	0.4
Dry	0 J/kg	1	0.8

Table 3: Estimates of the overturning timescale of the atmosphere in each of our three model cases.

Model	Layer mass	Mass Flux	Overturning time
Moist	7×10^{18} kg	6×10^{8} kg/s	371 years
Intermediate	4×10^{18} kg	2×10^{9} kg/s	64 years
Dry	3×10^{18} kg	4×10^{9} kg/s	24 years

Table 4: Observed (*Samuelson et al.* 1997) and modeled maximum northern spring equinoctial surface temperature differences between 60S and 60N latitude.

Model	Surface temperature gradient
Observations	$\sim$3 K
Moist	2 K
Intermediate	3.6 K
Dry	1.7 K
Dry R-C	24 K
Moist R-C	12 K

Table 5: Estimates of the phase lag with solar forcing (from Fig. 6) and amplitude of seasonal changes in temperatures (from Fig. 8) for our model simulations.

Model	Phase lag	Amplitude
Moist (<70N/S)	6 years	$\leq$ 3K
Moist (>70N/S)	0 years	$\leq$ 5K
Intermediate	2 years	$\leq$ 5K
Dry	0 years	$\leq$ 7K

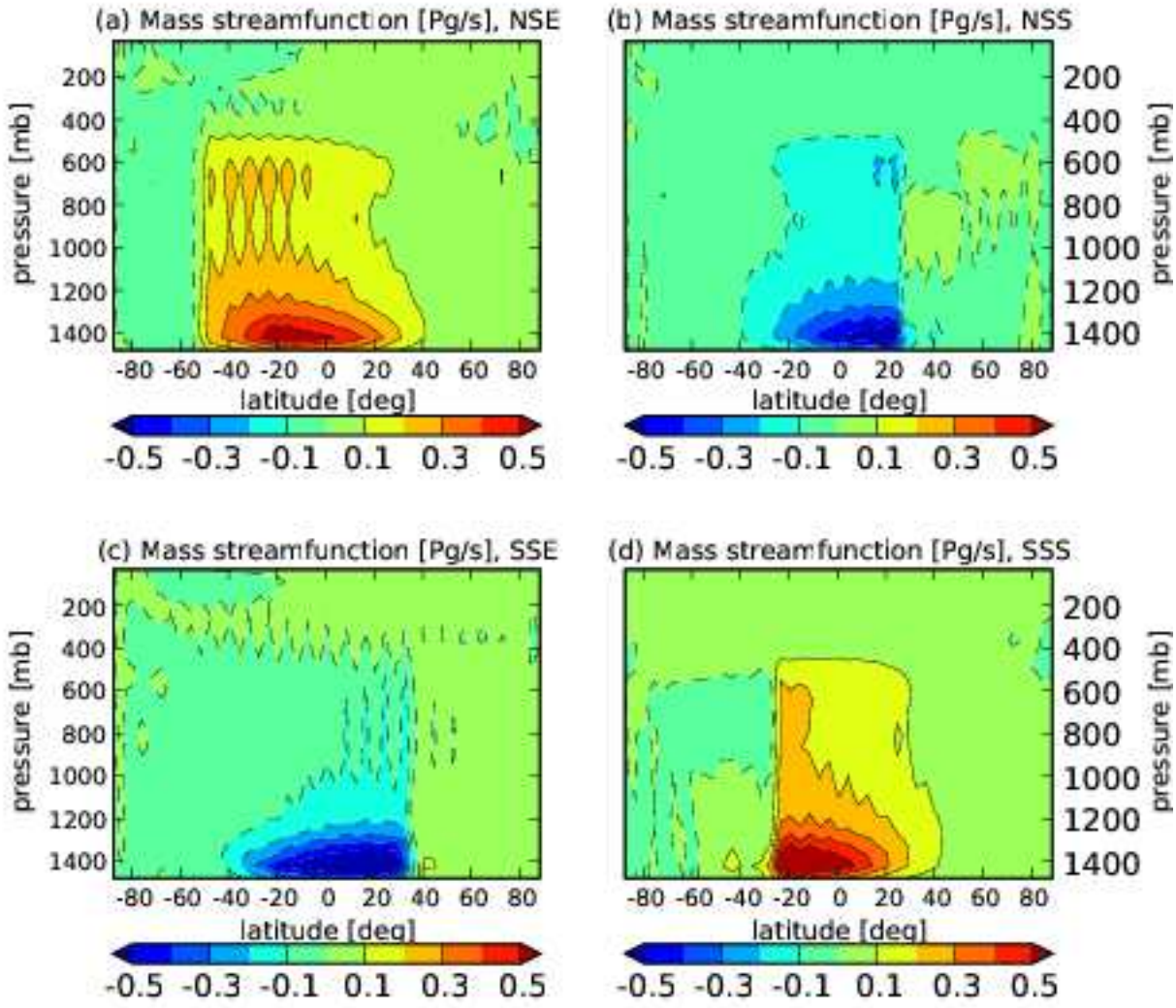

Fig. 1.— Mass streamfunction, or Hadley cell, for our moist case in Pg/s (10^{15}g/s) at each of the four seasons: [N/S]SE - northern/southern spring equinox; [N/S]SS - northern/southern summer solstice. The difference between adjacent contours of the mass streamfunction represents the mass flux in that region. In this and all subsequent plots, warm(cool) colors indicate clockwise(counter-clockwise) mass flux.

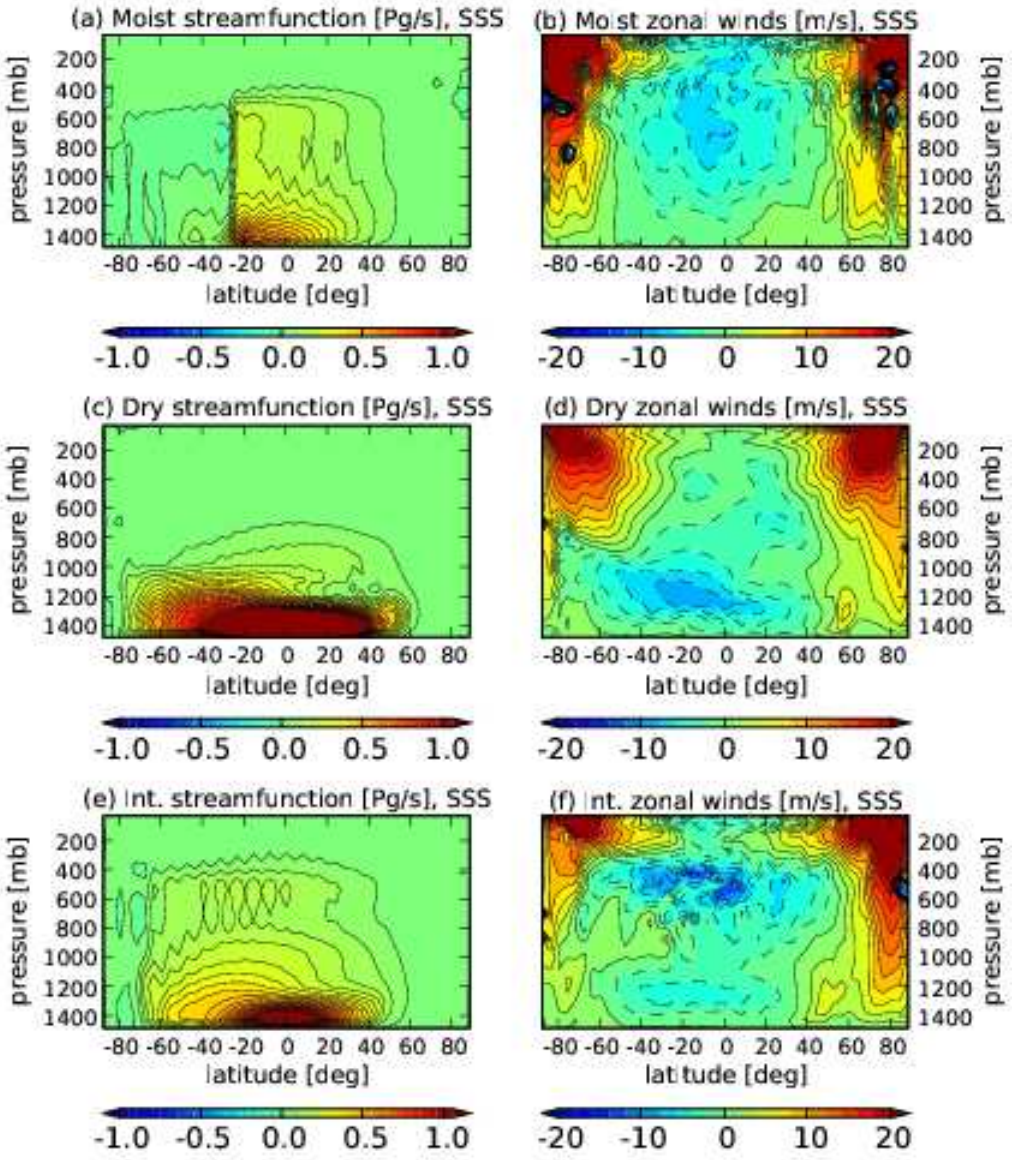

Fig. 2.— Streamfunction in Pg/s (10^{15}g/s) and zonal winds (m/s) at SSS. Warm(cool) contours indicate clockwise/westerly (counter-clockwise/easterly) mass fluxes and zonal winds. Streamfunction contours are spaced evenly from -20 to 20 pg/s in the moist case, -90 to 90 pg/s in the dry case, and -40 to 40 pg/s in the intermediate case. Contours for the zonal winds are all spaced between -20 to 20 m/s.

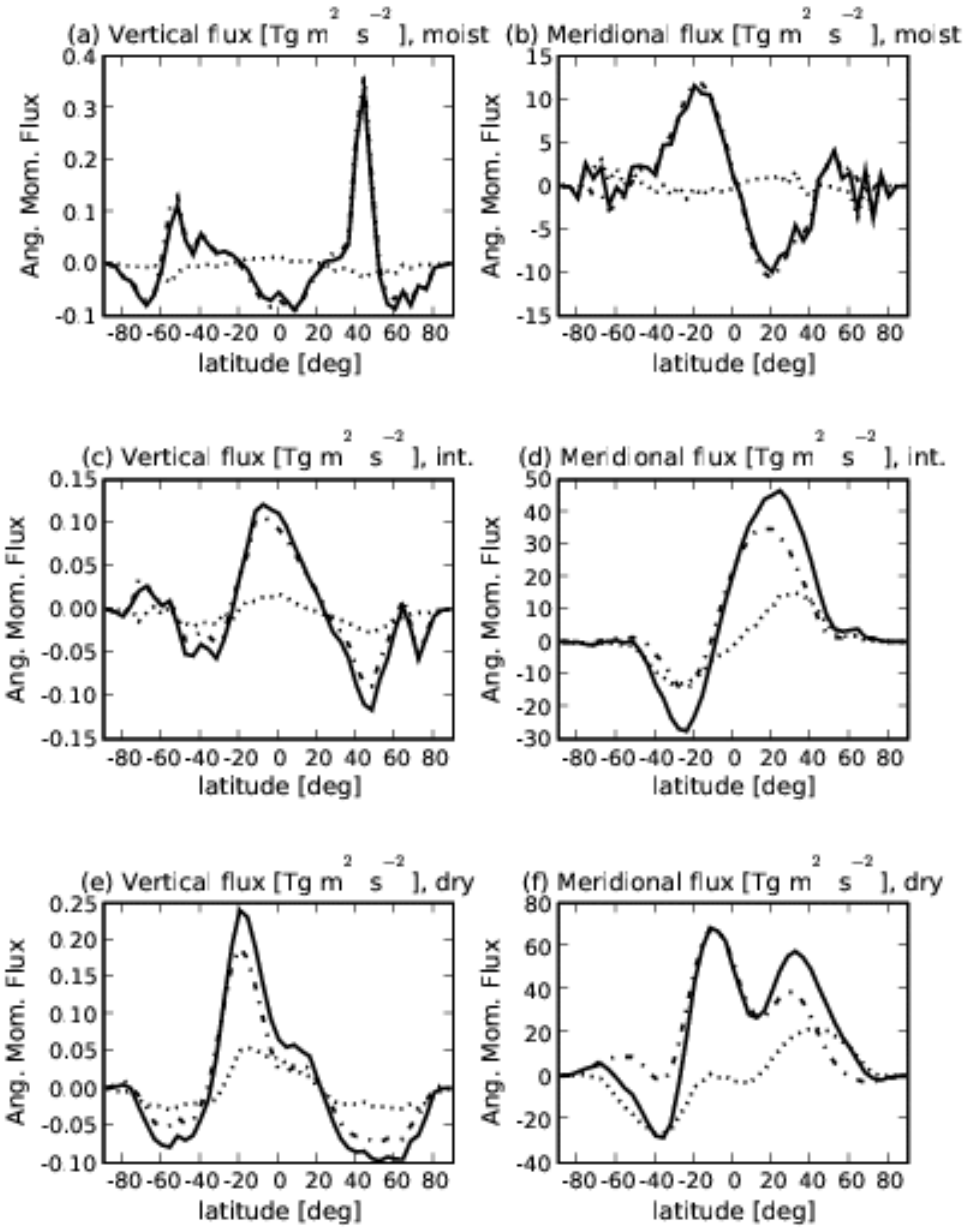

Fig. 3.— Annual-mean angular momentum fluxes in Tg (10^{12}g) m^2/s^2 averaged over the free troposphere (altitudes above 1360 mbar); vertical fluxes – left column, horizontal fluxes – right column. Each directional component is split into a time-variable term (dotted line) and mean-product term (dash-dotted line), as shown in Eq. 8. The total component fluxes are shown as the solid lines.

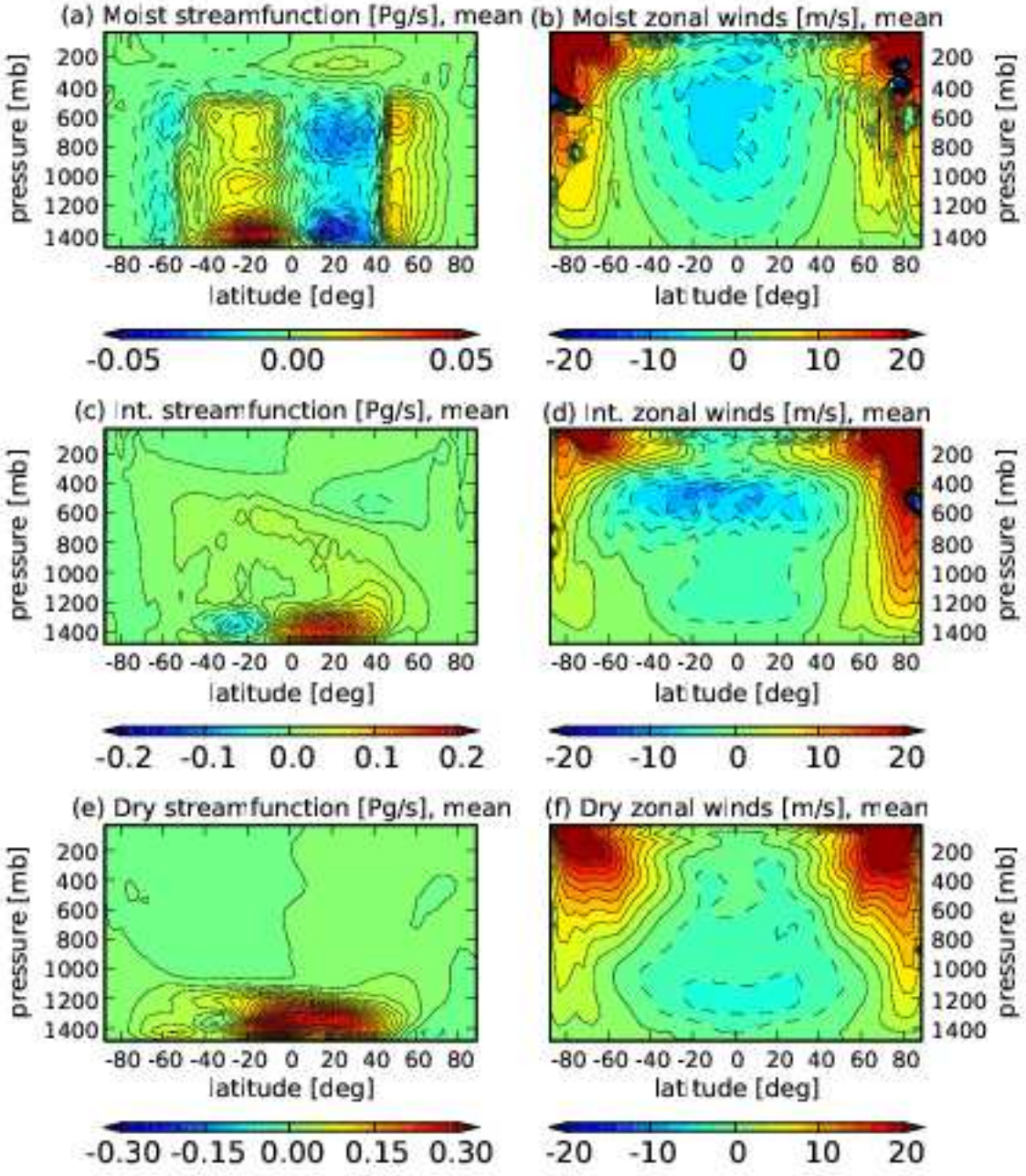

Fig. 4.— Annual-mean mass fluxes in Pg/s (10^{15}g/s, left column) and zonal winds in m/s (right column).

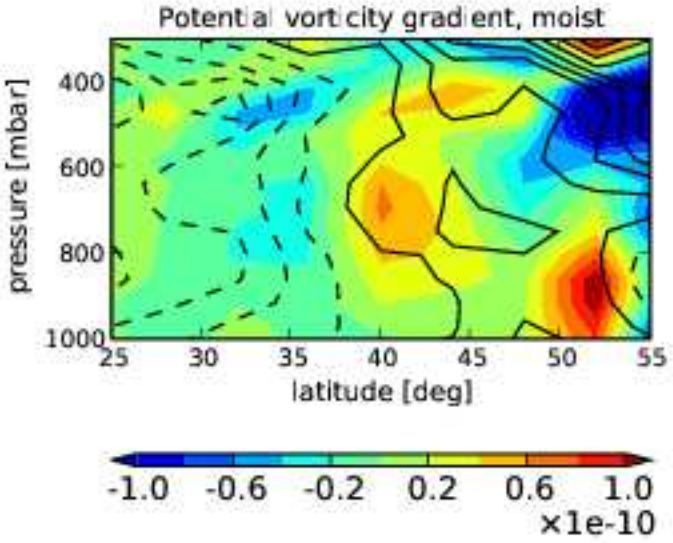

Fig. 5.— Potential vorticity gradient (shaded contours) and zonal winds (lines) in the moist case at SSS. Zonal wind contours are spaced at 1 m/s intervals from -10 to 10 m/s; solid (dashed) lines indicate positive (negative) zonal winds. The units of potential vorticity gradient is $(\mathrm{m\ s})^{-1}$.

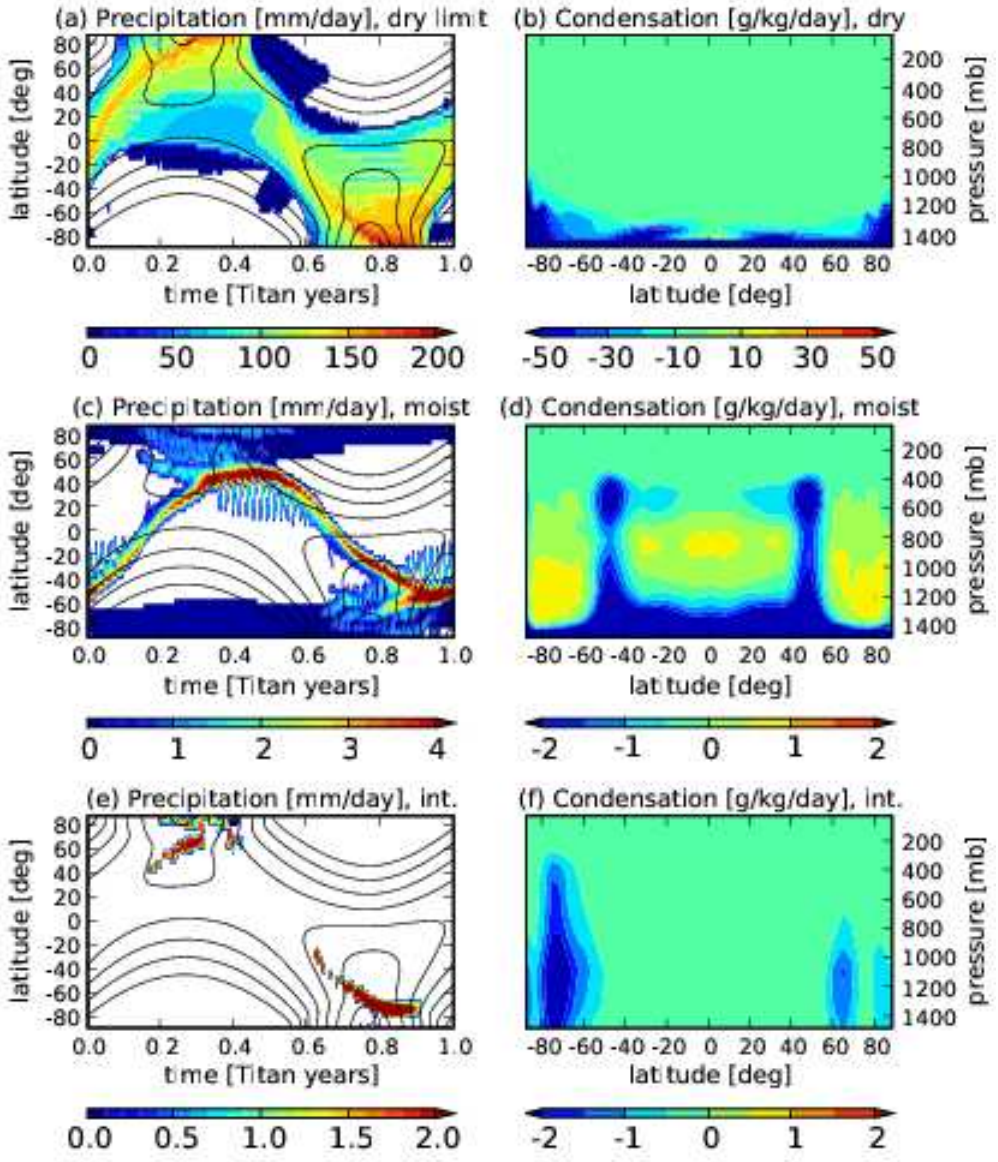

Fig. 6.— Left column: 10-Titan-day average precipitation in mm/day (filled contours) for our three simulations, with the pattern of solar forcing at the surface overlaid (black lines) for reference. Right column: Average convective drying in g/kg/day over 10(5) Titan years for the moist and intermediate (dry) cases. Note that since latent effects are ignored in the dry case, the units have no physical significance.

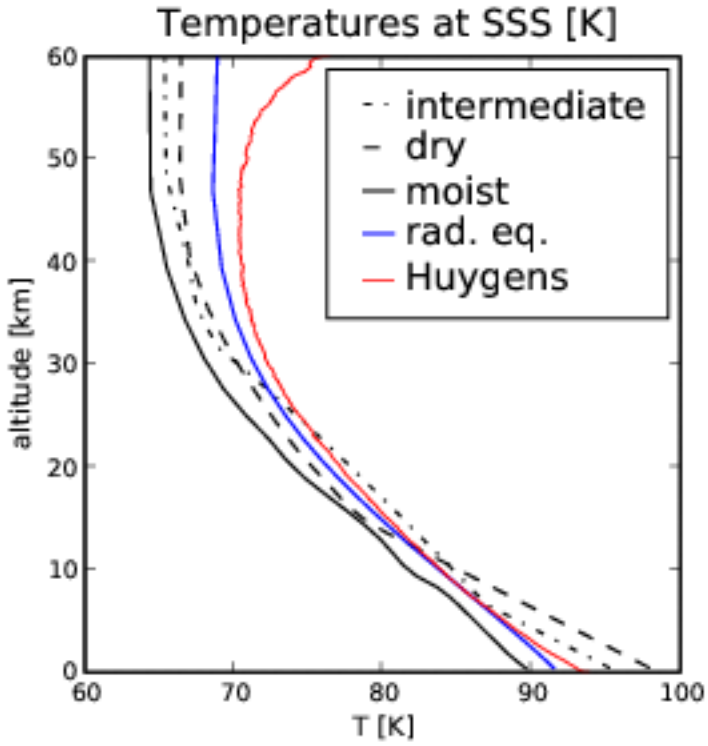

Fig. 7.— Vertical temperature profiles for our simulations at the Huygens epoch and 10S latitude compared with observations. The artificially warm model temperatures, which result from the neglect of the shielding by the stratospheric haze, are decreased by 15 K for comparison with the Huygens observation. Red line – Huygens observation; blue line – radiative equilibrium of our model; dotted line – temperatures extrapolated from the observed surface temperature along the dry adiabat; solid black line – moist simulation; dashed line – intermediate simulation; dot-dashed line – dry simulation.

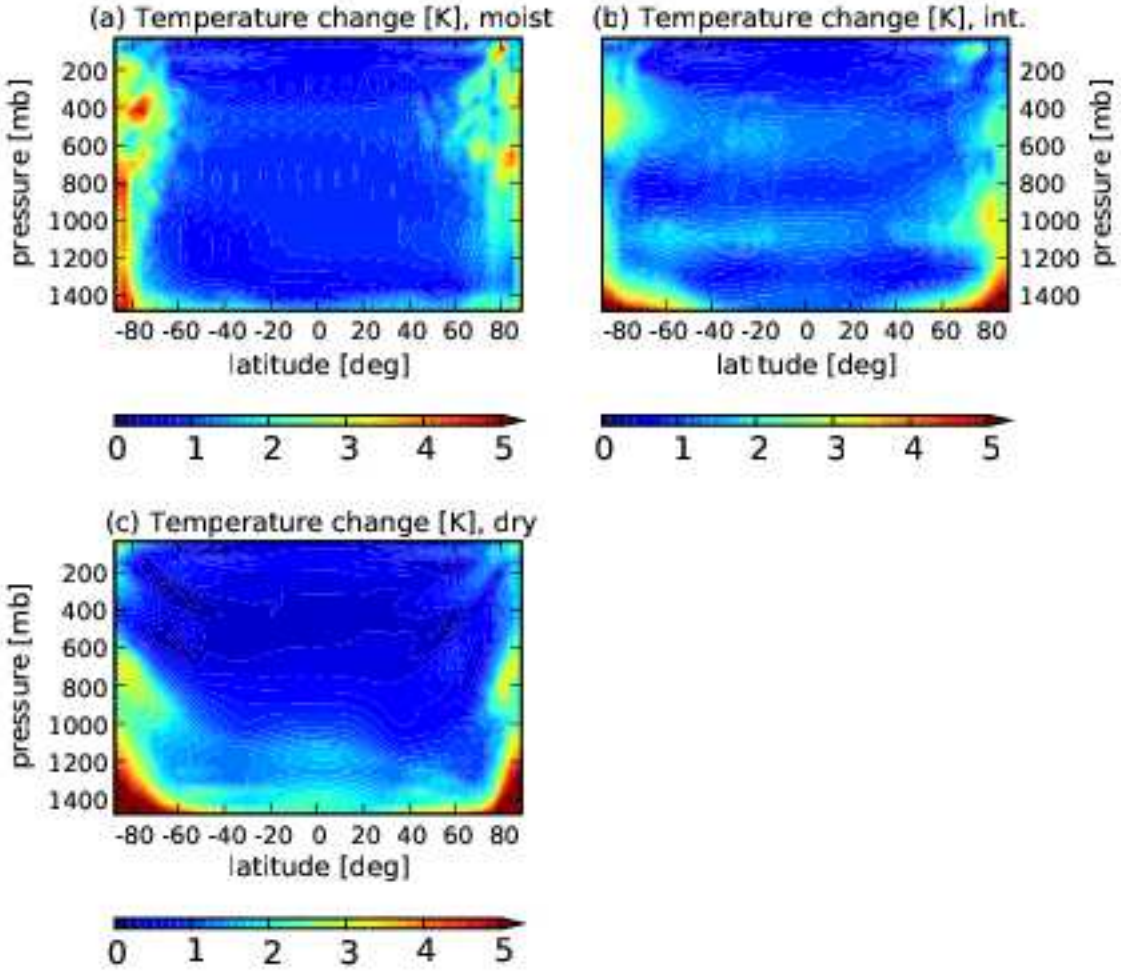

Fig. 8.— Amplitudes of the difference in temperature extrema in K over one Titan year in our three simulations. The largest difference occurs in the dry case, and is ∼7 K.

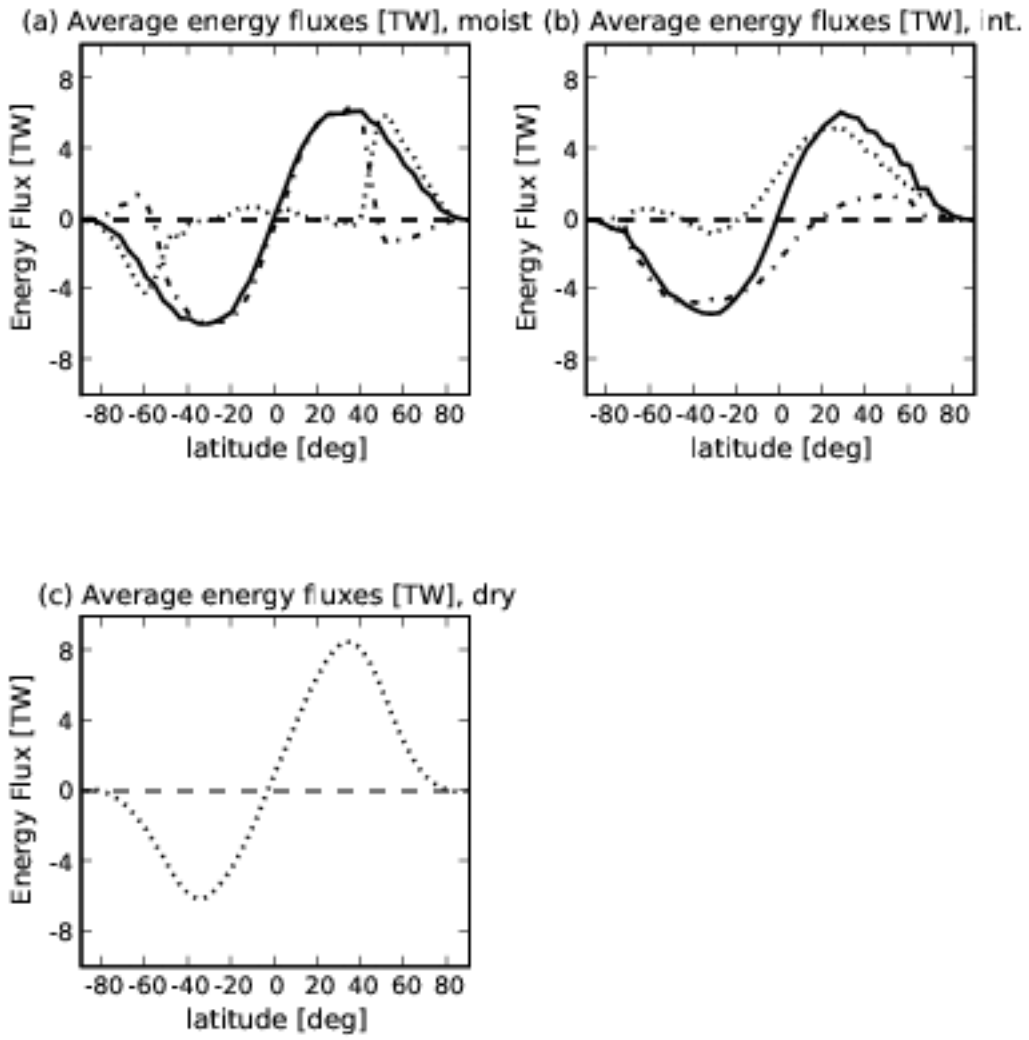

Fig. 9.— Energy fluxes in TW (10^{12}W) for each of our three cases: solid line - MSE flux; dash-dotted line - moisture flux; dotted line - DSE flux. The dry case has no moisture flux, therefore only the DSE flux is displayed.